



Selective binding to monoamine oxidase A: In vitro and in vivo evaluation of ^{18}F -labeled β -carboline derivatives



Hanno Schieferstein^a, Markus Piel^{a,*}, Friderike Beyerlein^a, Hartmut Lüddens^c, Nicole Bausbacher^b, Hans-Georg Buchholz^b, Tobias L. Ross^a, Frank Rösch^a

^aInstitute of Nuclear Chemistry, Johannes Gutenberg-University, 55128 Mainz, Germany

^bDepartment of Nuclear Medicine, University Medical Center Mainz, 55131 Mainz, Germany

^cDepartment of Psychiatry and Psychotherapy, University Medical Center Mainz, 55131 Mainz, Germany

ARTICLE INFO

Article history:

Received 26 July 2014

Revised 4 November 2014

Accepted 27 November 2014

Available online 8 December 2014

Keywords:

β -Carboline

Monoamine oxidase-A

Fluorine-18

μPET -study

Positron emission tomography

ABSTRACT

In this study we synthesized four different ^{18}F -labeling precursors for the visualization of the monoamine oxidase A using harmol derivatives. Whereas two are for prosthetic group labeling using [^{18}F]fluoro- d_2 -methyl tosylate and 2-[^{18}F]fluoroethyl-tosylate, the other three precursors are for direct nucleophilic ^{18}F -labeling. Additionally the corresponding reference compounds were synthesized. The syntheses of [^{18}F]fluoro- d_2 -methyl-harmol and 2-[^{18}F]fluoroethyl-harmol were carried out using harmol as starting material. For direct nucleophilic ^{18}F -labeling of the tracers carrying oligoethylened spacers (PEG), a toluene-sulfonyl leaving group was employed. The radiolabeling, purification and formulation for each tracer was optimized and evaluated in vitro and in vivo. Stability tests in human serum showed that all tracers were stable over the observation period of 60 min. μPET studies using of the synthesized tracers revealed that the tracers carrying PEG spacers showed no sufficient brain uptake. Consequently, the ^{18}F -fluoro alkylated tracers [^{18}F]fluoro- d_2 -methyl-harmol and 2-[^{18}F]fluoroethyl-harmol were further evaluated showing SUVs in the brain of $1.0 \pm 0.2 \text{ g/mL}$ and $3.4 \pm 0.5 \text{ g/mL}$ after 45 min, respectively. In blockade studies the selectivity and specificity of both tracers were demonstrated. However, for [^{18}F]fluoro- d_2 -methyl-harmol a rapid washout from the brain was also observed. In vitro binding assays revealed that 2-[^{18}F]fluoroethyl-harmol ($\text{IC}_{50} = 0.54 \pm 0.06 \text{ nM}$) has a higher affinity than the ^{18}F -fluoro- d_2 -methylated ligand ($\text{IC}_{50} = 12.2 \pm 0.6 \text{ nM}$), making 2-[^{18}F]fluoroethyl-harmol superior to the other evaluated compounds and a promising tracer for PET imaging of the MAO A.

© 2014 Elsevier Ltd. All rights reserved.

1. Introduction

In 1928, Mary Hare isolated an enzyme¹ called monoamine oxidase (MAO), which is responsible for the deamination of monoamines.^{2,3} This flavin-containing enzyme, located in the outer mitochondrial membrane,⁴ can be divided into two subtypes, MAO A and MAO B with 70% of amino acid sequence homology.^{5,6} The distribution of MAO varies throughout the human body and in animal models. Both isoforms occur in neuronal and non-neuronal cells⁷, but differ in their substrate specificity.^{8–11} MAO A degrades noradrenaline and serotonin, while MAO B is responsible for the deamination of phenethylamine and benzylamine (cf. Fig. 1).¹²

Dopamine and tyramine are metabolized by both isoforms.⁴ Thus, the monoamine oxidases are involved in the protection of neurons from exogenous amines, termination of the actions of

amine neurotransmitters and regulation of intracellular amine concentration. MAO is related to some psychiatric and neurodegenerative disorders, such as depression. Its role in Parkinson's

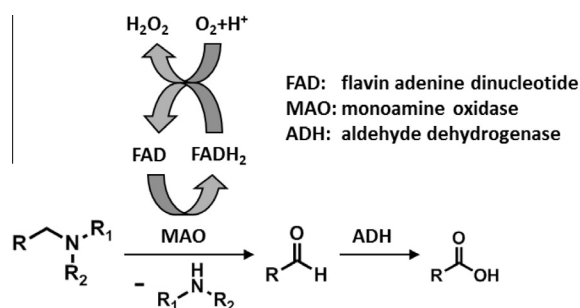


Figure 1. Proposed pathways of the degradation reactions of the MAO is involved in.

* Corresponding author. Tel.: +49 6131 3925701; fax: +49 6131 3926606.

E-mail address: piel@uni-mainz.de (M. Piel).

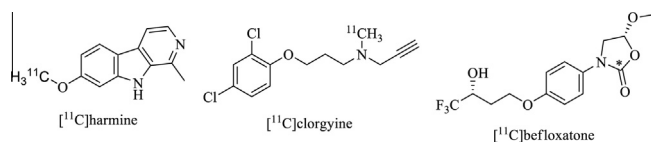


Figure 2. Commonly used ^{11}C -labeled MAO A tracers.

disease is well established.^{13–16} Depression is still under specific circumstances treated with MAO inhibitors, though this therapy approach leads to serious side effects like the ‘cheese reaction’.^{17–19}

Positron emission tomography (PET), as a non-invasive method to visualize enzyme concentrations *in vivo*, is a very efficient way to determine MAO levels in the brain. Hence, several ^{11}C -labeled tracers were developed to map MAO levels, like $[^{11}\text{C}]$ clorgyline, $[^{11}\text{C}]$ befloxadone or $[^{11}\text{C}]$ harmine (Fig. 2).^{20–22}

All of them have their drawbacks, like short biological half-lives, sophisticated syntheses or species differences in binding.^{23,24} Although harmine, a reversible MAO A inhibitor with a K_i value of 2 nM, shows an extensive metabolism in plasma, it is the most often used tracer for PET-studies.²⁵ Thus it would be desirable to obtain a ^{18}F -fluorinated analogue of $[^{11}\text{C}]$ harmine, due to the better isotopic properties of ^{18}F . In a previous study, Blom et al. synthesized fluoroalkylated and fluoropegylated harmine derivatives by varying the fluorinated moieties at the phenolic hydroxyl function.^{21,23,26} Initial autoradiographic experiments of rat brain slices have been performed showing promising results, like decreased non-specific binding in the brain, by using the ^{18}F -labeled harmine derivatives.²⁷

For the synthesis of ^{18}F -fluorinated analogues of ^{11}C -methylated tracers different strategies can be followed. One of these, the ^{18}F -fluoroethylation, is a convenient and very often used approach, although it may result in different biological properties of the ^{18}F -fluoroethylated tracer due to steric or lipophilic differences compared to a ^{11}C -methylated tracer.^{28,29} Recently, the ^{18}F -fluoromethylation has become an interesting alternative to the ^{18}F -fluoroethylation, since one major drawback of this method, the usually occurring fast metabolism of the ^{18}F -fluoromethylated compounds, can be often avoided by an alternative approach. By using $[^{18}\text{F}]$ fluoro- d_2 -methyl derivatives as labeling agents, the metabolism of the tracer is reduced, since the carbon-deuterium bond is six to ten times stronger than the carbon-hydrogen bond.^{30,31} Furthermore, in a previous study in our group a reliable and automated radiosynthesis of $[^{18}\text{F}]$ fluoro- d_2 -methyl tosylate ($[^{18}\text{F}]$ F- d_2 -MTos) was successfully developed, resulting in short reaction times, high radiochemical yields and a high radiochemical purity for this prosthetic group.³²

Hence, the aim of this study was to synthesize $[^{18}\text{F}]$ fluoro- d_2 -methyl-harmol ($[^{18}\text{F}]$ F- d_2 MH), 2- $[^{18}\text{F}]$ fluoroethyl-harmol ($[^{18}\text{F}]$ FEH) and the ^{18}F -fluorinated PEG-derivatives developed by Blom et al. and to evaluate their suitability to image the MAO A status *in vitro* and *in vivo*.

2. Materials and methods

All reagents and solvents were of analytical-grade quality and purchased from Sigma–Aldrich, Acros, Fluka or Merck. Unless otherwise noted, all chemicals were used without further purification. 2-Fluoroethyl-tosylate was prepared according to a published procedure.³³ ^1H and ^{13}C spectra were recorded on a Bruker AC-300-Spectrometer. 400 MHz ^1H spectra were recorded on a DIX-400-Spectrometer. ^1H shifts were given in ppm with reference to the internal tetramethylsilane (TMS) standard. Electro-spray mass spectra (ESI) were recorded on a ThermoQuest Navigator Instrument (Thermo Electron). High resolution mass spectra (HRMS) were obtained on a Q-TOF-Ultima 3-Instrument (Waters). Column

chromatography was performed using Acros silica gel (0.040–0.063 nm). For thin-layer chromatography (TLC) Merck silica gel 60 F254 plates were used for detection at 254 nm. The microwave-supported syntheses were carried out using a commercially available CEM Discover. Semipreparative HPLC was performed on a Dionex P680A pump, a Raytest NaI scintillation counter (Gabi) and a Dionex UVD 170U (254 nm) absorbance detector using a set of Phenomenex Synergi C12 Max-RP columns (4 μm , 250 \times 10 mm). Dionex Chromleon software was used for UV-data analysis and Raytest Gina star software for radioactivity detection. For the purification all tracers a stepwise gradient elution system composed of 50 mM ammonium formate buffer as solvent A and acetonitrile as solvent B (initial A/B = 70:30, 7 min 70:30, 15 min 60:40, 22 min 50:50, 28 min 30:70), flow rate of 5 mL/min, was used. Radioanalytical HPLC was performed using an isocratic system of 65% acetonitrile and 35% 50 mM ammonium formate buffer with a flow rate of 1 mL/min.

2.1. Synthesis of reference compounds and precursors

2.1.1. Synthesis of harmol (2)

The demethylation of harmine was performed in accordance to Bergström et al.²⁶ In brief, to a solution of 2 g (9.5 mmol) harmine (**1**) in 60 mL of glacial acid 12.5 mL of hydrobromic acid were added slowly and refluxed for 24 h. The crude reaction mixture was evaporated to dryness and suspended in water. After addition of 1 M potassium hydroxide solution the precipitate dissolved completely. The aqueous phase was washed two times with dichloromethane and two times with ether and the final product precipitated after addition of 15 mL of a saturated ammonium chloride-solution. The precipitate was isolated by filtration and subsequently freeze-dried to give 1.55 g (7.8 mmol, 82%) of a pale green solid. ^1H NMR (300 MHz, CDCl_3) δ [ppm] = 11.419 (s, 1H), 8.143 (d, 1H), 8.047 (d, 1H), 7.793 (d, 1H), 7.003–6.806 (dd, 1H), 2.788 (s, 3H). ESI-MS (ESI⁺): m/z : 199.09 ([M+1]⁺).

2.1.2. Synthesis of fluoro- d_2 -methyl-harmol (3)

200 mg (1 mmol) of harmol (**2**) were dissolved in dry acetonitrile under Schlenk conditions. Then potassium *tert*-butoxide (112.2 mg, 1 mmol) was added in one portion and the solution stirred for 15 min at RT. 137 μL (1 mmol) diiodo- d_2 -methane were added and stirred for another 2 h at RT. After addition of 4 mL of a 1 M TBAF solution in THF the reaction turned brownish and was allowed to react for 18 h at RT. The solvent was removed under vacuo and the residue purified by column chromatography (DCM/MeOH 15:1 + 2% TEA). The product fractions were combined, the solvent evaporated, redissolved in 10 mL dichloromethane and washed with 10 mL of a 1 M NaHCO_3 solution. The organic layer was separated, dried over Na_2SO_4 and eluted over a SepPak Silica Plus cartridge, to trap the product. Then the cartridge was eluted with 20 mL ethyl acetate and the solvent evaporated *in vacuo*, to obtain 30 mg (0.13 mmol, 13%) of fluoro- d_2 -methyl-harmol. ^1H NMR (300 MHz, CDCl_3) δ [ppm] = 8.172 (d, 1H), 7.884 (d, 1H), 7.736 (d, 1H), 7.070 (d, 1H), 6.862–6.826 (dd, 1H), 2.909 (s, 3H). ^{13}C NMR (75 MHz, CDCl_3) δ [ppm] = 162.441, 146.267, 136.622, 134.151, 132.683, 127.616, 123.352, 113.887, 113.797, 113.242, 95.418, 84.204, 70.769, 70.634, 70.485, 70.230, 69.495, 67.950, 45.953, 16.329. HR-ESI-MS (ESI⁺): m/z : 377.1861 [M+1]⁺; 378.2017 [M+2]⁺.

2.1.3. Synthesis 2-fluoroethyl-harmol (4)

To a solution of 100 mg (0.5 mmol) harmol (**2**) in 10 mL dry ethanol, 97 mg (0.7 mmol) K_2CO_3 were added in one portion and stirred for 15 min at RT. Then 87.2 mg (0.5 mmol) of 2-fluoroethyl tosylate in 5 mL dry ethanol were added and the reaction heated to 70 $^\circ\text{C}$ for 18 h before the ethanol was evaporated. The crude

reaction mixture was purified by column chromatography (DCM/MeOH 10:1 + 2% TEA) yielding 56 mg (0.23 mmol, 46%) of a slightly yellow solid. ^1H NMR (300 MHz, CDCl_3) δ [ppm] = 11.434 (s, 1H), 8.152 (d, 1H), 8.077 (d, 1H), 7.813 (d, 1H), 7.026 (d, 1H), 6.88 (dd, 1H), 4.885 (t, 1H), 4.726 (t, 1H), 4.393 (t, 1H), 4.292 (t, 1H), 2.712 (s, 3H). ESI-MS (ESI⁺): m/z : 245.10 ([M+1]⁺).

2.1.4. General procedure for the synthesis of the oligoethylated compounds (PEG2, PEG3; 6a, 6b)

The syntheses of the ditosylated spacers were performed using a modified protocol of Mohler et al.³⁴ Hence, to a solution of 20 mmol of the respective oligoethylene glycol **5a** or **5b** in 10 mL of dry dichloromethane 50 mmol of toluenesulfonyl chloride were added in one portion and the mixture cooled to 0 °C. Then 44 mmol of DABCO, dissolved in 8 mL dichloro methane, were added slowly through a dropping funnel. The reaction mixture was allowed to stir for additional 3 h at RT and finally filtered. The filtrate was washed three times with water, the organic phase dried over sodium sulfate and the solvent removed under vacuo to give a pale yellow oil. To the crude reaction mixture 10 mL of dichloromethane were added to dissolve the oil. Addition of diethyl ether led to precipitation of the ditosylated oligoethylene glycols **6a** and **6b** as colorless crystals (yield: 70–85%).

2.1.4.1. Diethylenglycol ditosylate (6a). ^1H NMR (300 MHz, CDCl_3) δ [ppm] = 7.580 (d, 4H), 7.039 (d, 4H), 3.448 (t, 4H), 3.567 (t, 4H), 2.200 (s, 6H).

2.1.4.2. Triethylenglycol ditosylate (6b). ^1H NMR (300 MHz, CDCl_3) δ [ppm] = 7.77 (d, 4H), 7.33 (d, 4H), 4.11 (t, 4H), 3.64 (t, 4H), 3.50 (s, 4H), 2.42 (s, 6H).

2.1.5. General procedure for the synthesis of the oligoethylated harmol precursors (7a, 7b, 7c)

To a solution of 0.5 mmol harmol (**2**) in 15 mL dry acetone and 2 mL DMSO 0.75 mmol of sodium carbonate were added and stirred at RT. After 15 min 2 mmol of the respective ditosylate **6a**, **6b** or **6c**, dissolved in 10 mL dry acetone, were added. The reaction mixture was refluxed overnight, quenched with water and three times extracted with 20 mL of dichloromethane. The organic phase was dried over sodium sulfate and evaporated to dryness. The crude reaction mixture was purified by column chromatography (EA + 2% TEA). The combined fractions were evaporated, dissolved in dichloromethane and washed with 1 M sodium bicarbonate solution. The organic layer was dried over sodium sulfate and evaporated giving 55–75% yield for each particular compound.

2.1.5.1. 7-[2-(2-Tosylethoxy)ethoxy]-1-methyl-9H- β -carboline (7a). ^1H NMR (300 MHz, CDCl_3) δ [ppm] = 8.23 (d, 1H), 7.87 (d, 1H), 7.73 (d, 2H), 7.65 (d, 1H), 7.22 (d, 2H), 6.99 (s, 1H), 6.79 (dd, 1H), 4.13 (t, 2H), 4.02 (t, 2H), 3.72–3.66 (m, 4H), 2.74 (s, 3H), 2.31 (s, 3H). ^{13}C NMR (75 MHz, CDCl_3) δ [ppm] = 159.66, 145.02, 142.13, 141.37, 137.99, 134.96, 132.57, 129.86, 128.96, 128.34, 127.85, 125.98, 122.37, 115.72, 112.13, 110.11, 95.96, 69.92, 69.41, 68.73, 67.82, 21.55, 20.08. (ESI⁺): m/z : 441.18 ([M+1]⁺). HR-ESI-MS (ESI⁺): m/z : 441.1470 [M+1]⁺; 442.1551 [M+2]⁺; 443.1558 [M+3]⁺.

2.1.5.2. 7-[2-[2-(2-Tosylethoxy)ethoxy]ethoxy]-1-methyl-9H- β -carboline (7b). ^1H NMR (300 MHz, CDCl_3) δ [ppm] = 8.924 (s, 1H), 8.281 (d, 1H), 7.916 (d, 1H), 7.765 (d, 2H), 7.675 (d, 1H), 7.282 (d, 2H), 7.009 (d, 1H), 6.871 (dd, 1H), 4.166–4.120 (m, 4H), 3.823 (t, 2H), 3.690–3.519 (m, 6H), 2.740 (s, 3H), 2.378 (s, 3H). ^{13}C NMR (75 MHz, CDCl_3) δ [ppm] = 160.32, 144.94, 142.92, 140.07, 134.45, 132.74, 129.84, 128.93, 127.89, 125.95, 122.55, 115.19, 112.24, 110.94, 98.09, 95.85, 70.78, 69.66, 69.38, 68.68,

67.83, 21.60, 19.08. (ESI⁺): m/z : 485.19 ([M+1]⁺). HR-ESI-MS (ESI⁺): m/z : 485.1755 [M+1]⁺; 486.1790 [M+2]⁺; 487.1834 [M+3]⁺.

2.1.5.3. 7-(2-[2-[2-(2-Tosylethoxy)ethoxy]ethoxy]ethoxy)-1-methyl-9H- β -carboline (7c). ^1H NMR (300 MHz, CDCl_3) δ [ppm] = 8.277 (d, 1H), 7.912 (d, 2H), 7.700 (q, 3H), 7.252 (d, 1H), 7.000 (d, 1H), 6.865–6.829 (dd, 1H), 4.173 (t, 2H), 4.139 (t, 2H), 3.865 (t, 2H), 3.675–3.568 (m, 10H), 2.735 (s, 3H), 2.366 (s, 1H). ^{13}C NMR (75 MHz, CDCl_3) δ [ppm] = 159.82, 144.86, 142.26, 141.06, 137.55, 134.83, 132.71, 129.79, 127.83, 125.97, 122.35, 115.54, 112.04, 109.99, 95.80, 70.72, 70.67, 70.59, 70.46, 69.67, 69.29, 68.58, 67.72, 21.56, 19.97. ESI-MS (ESI⁺): m/z : 529.26 ([M+1]⁺). HR-ESI-MS (ESI⁺): m/z : 529.2018 [M+1]⁺; 530.2124 [M+2]⁺; 531.2052 [M+3]⁺.

2.1.6. General procedure for the synthesis of the oligoethylated reference compounds (8a, 8b, 8c)

The syntheses of the reference compounds were performed in analogy to Blom et al.²⁷ 0.02 mmol of **7a**, **7b** or **7c** were dissolved in 6 mL dry THF before 0.02 mmol of a 1 M TBAF solution in THF were added and heated at 55 °C. After 3 h the solvent was removed to afford the crude product. Chromatography of the residue ($\text{CHCl}_3/\text{MeOH}$, 8:1 + 2% TEA) gave the pure product with a yield of 40–50%.

2.1.6.1. 7-[2-(2-Fluoroethoxy)ethoxy]-1-methyl-9H- β -carboline (8a). ^1H NMR (300 MHz, CDCl_3) δ [ppm] = 8.173 (d, 1H), 7.897 (d, 1H), 7.693 (d, 1H), 6.979 (d, 1H), 6.860 (dd, 1H), 4.204 (t, 1H), 4.169 (t, 1H), 4.120 (m, 2H), 3.949 (m, 2H), 3.935 (m, 2H), 2.812 (s, 3H).

2.1.6.2. 7-[2-[2-(2-Fluoroethoxy)ethoxy]ethoxy]-1-methyl-9H- β -carboline (8b). ^1H NMR (300 MHz, CDCl_3) δ [ppm] = 9.321 (s, 1H), 8.276 (d, 1H), 7.911 (d, 1H), 7.682 (d, 1H), 6.943 (d, 1H), 6.863 (dd, 1H), 4.611 (t, 1H), 4.452 (t, 1H), 3.828 (m, 4H), 3.717 (m, 6H), 2.757 (s, 3H).

2.1.6.3. 7-(2-[2-[2-(2-Fluoroethoxy)ethoxy]ethoxy]ethoxy)-1-methyl-9H- β -carboline (8c). ^1H NMR (300 MHz, CDCl_3) δ [ppm] = 8.172 (d, 1H), 7.884 (d, 1H), 7.736 (d, 1H), 7.070 (d, 1H), 6.862–6.826 (dd, 1H), 4.579 (t, 1H), 4.406 (t, 1H), 4.155 (t, 2H), 4.124 (t, 2H), 3.755–3.551 (m, 10H), 2.909 (s, 3H). ^{13}C NMR (75 MHz, CDCl_3) δ [ppm] = 162.441, 146.267, 136.622, 134.151, 132.683, 127.616, 123.352, 113.887, 113.797, 113.242, 95.418, 84.204, 70.769, 70.634, 70.485, 70.230, 69.495, 67.950, 45.953, 16.329. HR-ESI-MS (ESI⁺): m/z : 377.1861 [M+1]⁺; 378.2017 [M+2]⁺.

2.2. Radiosyntheses

2.2.1. Radiosynthesis of [¹⁸F]fluoro-*d*₂-methyl-harmol (**9**)

[¹⁸F]F-*d*₂-MT was synthesized from n.c.a. [¹⁸F]fluoride (6–8 GBq) in an automated synthesis module as described in the literature and finally trapped on Strata™ X SPE cartridge (Phenomenex) and dried with helium.³² The [¹⁸F]F-*d*₂-MT was eluted into a reaction vial using 0.7 mL DMSO, tempered at 120 °C and added to a solution of 3 mg (15 μmol) harmol and 5.6 μL of a 5 N NaOH solution in 0.3 mL DMSO. The mixture was heated for 20 min at 110 °C. After cooling, the solution was diluted with 1 mL of the HPLC solvent mixture and the [¹⁸F]F-*d*₂-MT purified by semipreparative HPLC. The product fraction was diluted with water (25 mL), trapped on a Strata™ X SPE cartridge (Phenomenex), washed with 10 mL water, dried in a helium stream and eluted with 1 mL ethanol. The solvent was evaporated in vacuo and the residue dissolved in 0.4 mL isotonic saline solution to obtain the [¹⁸F]fluoro-*d*₂-methyl-harmol (0.8–1.2 GBq) after a synthesis time of 115 min in

an overall radiochemical yield of about $35 \pm 5\%$ with a high radiochemical purity of $>97\%$.

2.2.2. Radiosynthesis of 2- ^{18}F fluoroethyl-harmol (**10**)

2- ^{18}F fluoroethyl-tosylate (^{18}F FETos) was synthesized from n.c.a. ^{18}F fluoride (3–5 GBq) using a homemade automated synthesis module as described elsewhere and finally trapped on a Strata™ X SPE cartridge (Phenomenex) and dried with helium.³⁵ The ^{18}F FETos was eluted into a reaction vial with 0.8 mL DMSO, tempered at 130°C and added to a solution of 3 mg (15 μmol) harmol and 5.6 μL of a 5 N NaOH solution in 0.2 mL DMSO. The mixture was heated for 10 min at 130°C . After cooling, the solution was diluted with 1 mL water and the 2- ^{18}F fluoroethyl-harmol purified by semipreparative HPLC. The product fraction was diluted with water (25 mL), trapped on a Strata™ X SPE cartridge (Phenomenex), washed with 10 mL water, dried in a helium stream and eluted with 2 mL ethanol. The solvent was evaporated in vacuo and the residue dissolved in 1.0 mL isotonic saline solution to obtain the tracer (1.2 GBq) after a synthesis time of 100 min in an overall radiochemical yield of about $47 \pm 2\%$ with a high radiochemical purity of $>97\%$.

2.2.3. Radiosyntheses of the PEGylated compounds (PEG2–PEG4)(**11a–c**)

The PEGylated harmol derivatives were synthesized starting from n.c.a. ^{18}F fluoride (3–5 GBq) by a ^{18}F -direct fluorination in a micro wave oven. The aqueous ^{18}F fluoride solution was trapped on a Sep-Pak Accell Plus QMA light cartridge and eluted with a solution of 15 μL 1 M K_2CO_3 and 15 mg Kryptofix®222 in 0.8 mL MeCN. The water was removed using a stream of N_2 at 80°C and coevaporated to dryness with MeCN (3 \times 1 mL). Afterwards, the dried K^{18}F -K₂₂₂ complex was dissolved in 400 μL acetonitrile and added to a solution containing 2.8 μmol of the respective precursor (**7a,7b** or **7c**) in 200 μL acetonitrile. The reaction vial was sealed and placed in a microwave, heated for 5 min at 125°C and quenched with water. The crude product was purified via semipreparative HPLC using the conditions described above. The isolated tracer was diluted with water (25 mL), trapped on a Strata™ X SPE cartridge (Phenomenex), washed with 10 mL water and eluted with 2 mL of ethanol. The solvent was evaporated in vacuo and the residue dissolved in 1.0 mL isotonic saline solution to obtain the tracer (1 GBq) after a synthesis time of 85 min in an overall radiochemical yield of about $20 \pm 10\%$ with a high radiochemical purity of $>97\%$.

2.3. Plasma stability

3–5 MBq of ^{18}F F-*d*₂-MH (**9**), ^{18}F FEH (**10**), ^{18}F PEG2-harmol (**11a**), ^{18}F PEG3-harmol (**11b**) and ^{18}F PEG4-harmol (**11c**) in 200 μL saline solution were incubated in triplicates in 400 μL of human serum at 37°C . At 5, 20, 30 and 60 min the incubation was stopped by putting the Eppendorf vial on ice. Subsequently, 400 μL of MeCN were added to precipitate the plasma proteins and the vial was centrifuged at 10,000 rpm for 8 min. A sample of 20 μL of the supernatant was taken and analyzed in the radioanalytical HPLC system described above.

2.4. Animals

For all experiments Sprague Dawley rats (285 \pm 50 g) were used, which were obtained from the animal husbandry of the Johannes Gutenberg University of Mainz, Germany. Animals had access to food and water ad libitum. Temperature and humidity were kept at $24 \pm 2^\circ\text{C}$ and 60%, respectively. All animals were maintained on a 12-h light/12-h dark cycle. Handling occurred only during the light cycle. All animal experiments were performed in accor-

dance with the European Communities Council Directive of 24. November 1986 (86/609/EEC) and the German law for animal welfare and were approved by the local ethical committee for animal experiments.

2.5. In vivo imaging studies in Sprague Dawley rats

MicroPET imaging was performed with a Siemens/Concorde Microsystems microPET Focus 120 small-animal PET camera (Siemens/Concorde, Knoxville, TN, USA). Sprague Dawley rats were anaesthetized with 2.5% isoflurane in medical oxygen, placed in supine position in the small-animal PET scanner and warmed with a heating lamp. After cannulation of the tail vein, a 10 min transmission scan was performed using a ^{57}Co point source. Following an intravenous bolus injection of ^{18}F F-*d*₂-MH (26.2 ± 4.3 MBq) or ^{18}F FEH (28.5 ± 3.7 MBq) to wild type ($n = 5$), clorgyline treated rats ($n = 3$, 10 mg/kg clorgyline iv 10 min before injection of the tracer) and *l*-deprenyl treated rats ($n = 3$, 1 mg/kg *l*-deprenyl iv 10 min before injection of the tracer), a dynamic emission scan was accomplished for 1 h. Furthermore, for ^{18}F FEH challenge experiments in rats ($n = 3$) were performed using moclobemide, a reversible MAO A inhibitor with a K_i -value of 57.1 ± 5.2 μM .³⁶ Hence, following a published procedure 20 mg/kg moclobemide were injected in a bolus 20 min p.i. followed by a second injection of 10 mg/kg at 45 min p.i.³⁷ The ^{18}F -labeled PEGylated harmol derivatives were examined dynamically for 60 min in untreated animals ($n = 2$) after intravenous bolus injection (31.6 ± 2.4 MBq) of the tracer.

The obtained list-mode files were rebinned to sinograms with 19 frames (3 \times 20 s, 3 \times 60 s, 3 \times 120 s, and 10 \times 300 s) and reconstructed by four iterations of 2-dimensional ordered-subset expectation maximization (OSEM2D) with scatter and attenuation correction. This finally results in a $128 \times 128 \times 95$ matrix, with $0.87 \times 0.87 \times 0.80$ mm³ voxels. Reconstructed images were analyzed with the modeling computer software PMOD (PBAS & PFUS, PMOD Technologies Ltd, Zurich, Switzerland). Using the summed PET images (0–60 p.i.) the brain was co-registered to a MRI template (93 \times 93 \times 120 matrix) via rigid translations and rotations for each axis, till the PET image matches the MRI template. The obtained transformation matrix then was applied to each frame of the dynamic PET images, resulting in a PET study with a 93 \times 93 \times 120 matrix. Then a volume of interest (VOI) for the brain was drawn on the MRI template and applied to the PET images, to determine the time activity curve (TAC) of the brain uptake for each animal. Afterwards, the TAC of this VOI was decay corrected to the injection time and normalized concerning the injected dose and the weight of the animal to obtain the SUV [SUV = (radioactivity in Bq per mL/injected radioactivity in Bq) \times body weight in g] for each time point.

2.6. In vivo metabolism studies

The metabolism of ^{18}F F-*d*₂-MH (**9**) and ^{18}F FEH (**10**) was determined in analogy to Herth et al.³⁸ Briefly, blood samples were taken 5, 10, 20, 30, 60 min p.i. Erythrocytes and plasma proteins were precipitated and plasma water was measured using a Perkin-Elmer Wizard² auto-gamma counter.

2.7. Monoamine oxidase assays

Rat brain cortical membranes were obtained as previously described.³⁹ After thawing the membranes were centrifuged at 23,000g for 20 min and resuspended in 50 mM Tris/HCl, pH 7.5 (Tris/HCl).

The MAO assay was performed according to Krajl et al. with some modifications.⁴⁰ In brief: cortex membranes were

pre-incubated in Tris/HCl with 37.5 nM clorgyline and 37.5 nM α -deprenyl for 5 min at 37 °C to selectively and irreversibly inhibit MAO A and MAO B, respectively (Fig. 8). The range of compounds 1–4 and dopamine is given in the text. Total MAO activity was obtained in the absence of any additive and total nonspecific values were determined in the presence of 8.33 μ M pargyline. The volume during incubation amounted to 200 μ L. All assays were performed at least three times in duplicates.

Final protein concentrations were kept in the range from 50 μ g to 115 μ g in each tube in order to obtain little variation in the MAO-subtype irreversible inhibition by clorgyline and α -deprenyl, respectively.⁴¹ The reaction was started by the addition of 25 μ M kynuramine hydro bromide, slightly below the K_M value in order to avoid substrate inhibition.⁴² After 30 min at 37 °C the reaction was terminated by 267 mM HClO₄. Samples were centrifuged at 13,000g for 2 min and an aliquot of the supernatant was added to a four-fold excess in volume of 1 M NaOH. Data were normalized to the value in the presence of clorgyline (MAO-B) and α -deprenyl (MAO A), set to 100%. The sum of the thus determined values for MAO A activity and MAO B activity were around 100% of the total MAO activity for all assays. Fluorescence of the developed 4-OH-quinoline was measured in a Fluoromax 2 fluorescence spectrophotometer (Horiba Scientific, Unterhaching, Germany) at 313 nm absorption and 410 nm emission with slit widths of 2 nm. The IC₅₀ values were fitted to a sigmoidal dose-response curve using GraphPad (version 5).

3. Results and discussion

The main purpose of this study was to synthesize and evaluate ¹⁸F-fluorinated harmine derivatives for the in vivo visualization of the monoamine oxidase A with PET. A common approach for the synthesis of ¹⁸F-fluorinated derivatives is the ¹⁸F-fluoroalkylation of ¹¹C-labeling precursors, for example, giving 2-[¹⁸F]fluoroethyl-harmol. Moreover recent developments in ¹⁸F-fluoro-*d*₂-methylation techniques, enabled us to synthesize [¹⁸F]fluoro-*d*₂-methyl-harmol, which seems to be a promising candidate because of the similar steric demands of a fluoromethyl and a methyl moiety. New PEGylated harmine derivatives were also synthesized, because they seem to be interesting, due to the promising results of autoradiographic studies performed by Blom et al.²⁷ Particularly, it has been shown, that

replacing the methyl group of harmine by an oligoethylene glycol spacer (PEG2, PEG3) resulted in a decrease of unspecific tracer-binding. Consequently, we decided to synthesize and evaluate an additional PEG4 derivative of harmol to investigate the influence of all PEG spacers on the brain uptake and specific binding.

All reference compounds and the precursors of this lead structure were synthesized and reaction conditions for their labeling screened and optimized. Furthermore, the tracers were evaluated in plasma stability tests and μ PET imaging studies, as well as their affinity tested in binding assays.

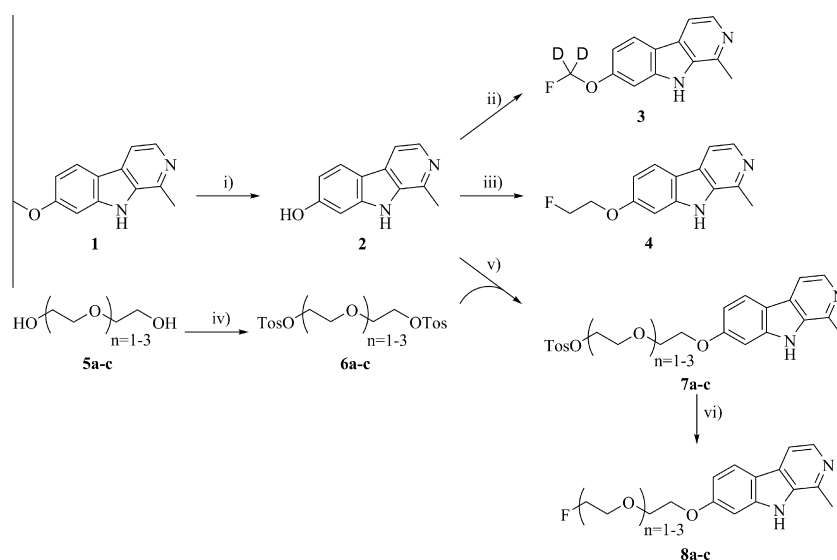
3.1. Synthesis of labeling precursors and reference compounds

The precursors and reference compounds were synthesized according to the routes shown in Scheme 1. The organic reactions were screened and optimized with regard to solvents, base, reaction temperature and side reactions, considering that the reactions follow a S_N2 mechanism.

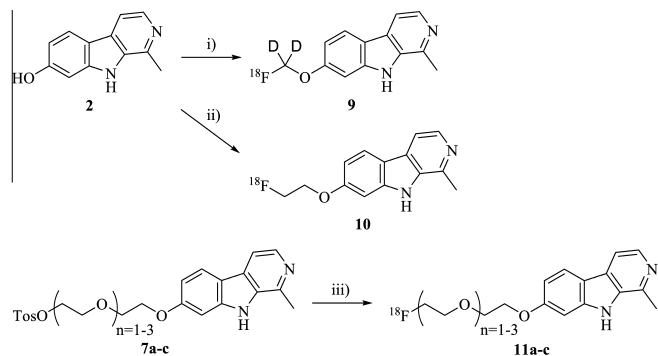
Harmol, the key intermediate of every synthesis, was prepared via demethylation of harmine (1) using HBr/glacial acid according to a published procedure²⁶, giving the harmol in high yields of about 80%. The synthesis of 2-fluoroethyl-harmol was performed in a similar manner by reacting harmol (2) with 2-fluoroethyl-tosylate in the presence of potassium carbonate as base and potassium iodide as catalyst, resulting in moderate yields of 46% for this reference compound (Scheme 2).

Possible synthetic routes for the preparation of the first reference compound, fluoro-*d*₂-methyl-harmol, were limited by the commercial availability of suitable deuterated methylating agents. Hence, a two-step procedure was examined, which consists of the alkylation of harmol with diiodo-*d*₂-methane, followed by a fluorination of the obtained iodo-*d*₂-methyl-harmol with tetra-*n*-butylammonium fluoride (TBAF). First attempts to purify the crude product of the alkylation step via column chromatography were unsuccessful, due to the decomposition of the iodo-*d*₂-methyl-harmol on the column. Thus, the reaction route was performed as a two-step one-pot synthesis, giving the fluoro-*d*₂-methyl-harmol in a high chemical purity and a yield of 13%.

Although the syntheses of the reference compounds and labeling precursors for the PEGylated compounds have already been described in the literature, the use of toluenesulfonyl moieties



Scheme 1. Synthesis routes of precursors and reference compounds. Reagents and conditions: (i) HBr/HAC; (ii) KOTu, CD₂I₂, TBAF; (iii) K₂CO₃, EtOH, FETos, 70 °C; (iv) DABCO, DCM, 0 °C; (v) Cs₂CO₃, DMSO, acetone, reflux; (vi) THF, TBAF, 55 °C.



Scheme 2. Radiosynthesis of harmol derivatives. Reagents and conditions: (i) [^{18}F]F- d_2 -MTos, 2 equiv 5 N NaOH; (ii) [^{18}F]FETos, 2 equiv 5 N NaOH; (iii) K^{18}F , K2.2.2/MeCN, microwave.

Table 1
Optimization of base systems for the coupling reaction of harmol and the PEG-spacers

Base	6a yield (%)	6b yield (%)	6c yield (%)
TMA	<1	nd	nd
DEA	7	5	10
TEA	18	15	20
K_2CO_3	36	42	65
Cs_2CO_3	15	20	28
NaH	17	20	10

for the oligoethylene spacer carrying tracers as leaving groups instead of halides was preferred for this study, to increase the radiochemical yields.²⁷ A further advantage of using toluenesulfonyl groups is the prolonged shelf-life of the precursors, which facilitates the storage of the precursors at 4 °C instead of -78 °C. In contrast to the tetraethylene glycol ditosylate (**6c**), which is commercially available, the ditosylated oligoethylene spacers diethylene glycol ditosylate (**6a**) and triethylene glycol ditosylate (**6b**) had to be synthesized using a modified protocol of Mohler et al.³⁴ Hence, the oligoethylene glycol spacers were ditosylated by using toluenesulfonyl chloride and DABCO instead of triethylamine, followed by precipitation of the products due to the addition of a huge excess of cold diethyl ether. For the following coupling reaction the different reaction parameters were screened and optimized (Table 1) because of the low yields achieved in previous studies.

The use of non-nucleophilic bases like trialkylamines or carbonates for this step was necessary to avoid side reactions. Whilst di- or trialkylamines (DEA, TEA) seemed to be less suitable, indicated by the low yields of up to 20%, the use of sodium hydride led almost exclusively to decomposition of the harmol (**2**). In contrast, the inorganic bases, like carbonates, showed the most promising results, especially potassium carbonate, which gave the highest yields in all three coupling reactions and a minimum of side reactions. However, the use of potassium or cesium carbonate led to by-products in all cases showing similar R_f -values compared to the desired products. Since these by-products were predominantly observed when strong bases were used for this reaction, the by-products of a reaction of **6c** and harmol in the presence of cesium carbonate were examined. The characterization of the side product via NMR- and mass-spectroscopy showed, that an *N*-alkylation of harmol took place. To verify that hypothesis, that *N*-alkylation is possible, a *N*-Boc-protected harmol derivative was synthesized and reacted with PEG4-ditosylate under the same reaction conditions, indicating no formation of the by-product. Beside the base screening, different solvent systems were tested to facilitate the whole work-up procedure and thus avoiding high boiling solvents (Table 2).

Table 2
Optimization of solvents for the coupling reaction of harmol and the PEG-spacers

Solvent	DMF	DMSO/acetone	DCM	CHCl_3	DMSO
Yield (%)	15	71	22	0	65

The focus of the whole optimization process was set on the reactions using PEG4 (**6c**), because this synthesis gave the best yields during the base screening process. Unfortunately, this screening showed that a mixture of DMSO and acetone was superior to solvents like DMF, pure DMSO and dichloromethane. Thus, it was only possible to reduce the amount of high boiling solvents, to simplify the purification of the products.

In summary, the optimization showed that potassium carbonate and a mixture of acetone/DMSO as base and solvent were the system of choice, and hence were used for the general synthesis procedure for the preparation of precursors **7a**, **7b** and **7c**. Furthermore, compared to a previous study, the yields of the precursors were increased significantly, by using the ditosylated PEG-spacers and the reaction conditions described above. The fluorination steps for the synthesis of the reference compounds were performed following a general procedure using a 1 M TBAF solution in THF, whereas no optimization was carried out.²⁷ These reactions proceeded without any side reactions, requiring no special workup procedure, and gave the reference compounds in good yields.

3.2. Radiochemistry

The radiolabeling of the different precursors was performed as shown in Scheme 2.

The synthesis of [^{18}F]fluoro- d_2 -methyl-harmol was performed in a two-step procedure. In the first step, the labeling agent [^{18}F]fluoro- d_2 -methyl tosylate was produced, which was then used to [^{18}F]fluoro methylate harmol. Therefore, the [^{18}F]fluoro- d_2 -methyl-harmol was produced in an automated synthesis module. According to a recently published study the [^{18}F]labeled prosthetic group could be obtained after a synthesis time of 50 min in a radiochemical yield of about 45%.³² For the next step the [^{18}F]F- d_2 -MTos, which was finally trapped on a Strata-X 33 μM SPE cartridge and eluted with DMSO, was tempered to the reaction temperature. Then it was reacted with a solution of harmol and 5 N NaOH in DMSO to obtain the final [^{18}F]F- d_2 -MH. For the labeling reaction different reaction parameters, like precursor concentration, amount of base, reaction time and temperature were optimized, resulting in the following reaction conditions: 15 μmol harmol, 5.6 μL 5 N NaOH, 110 °C and 20 min reaction time. This gave radiochemical yields of about 80% for the [^{18}F]fluoromethylation step. The purification of the reaction mixture was performed by HPLC, trapping the product on SPE cartridge, elution with ethanol, evaporation of the ethanol and subsequent formulation in isotonic sodium chloride solution, yielding the [^{18}F]F- d_2 -MH in an overall radiochemical yield of about 35% after a synthesis time of 115 min and specific activities of 40–90 GBq/ μmol .

In a first approach to synthesize [^{18}F]fluoroethyl harmol via a [^{18}F]direct fluorination, a precursor from a previous study,²⁷ 2-(1-methyl-9H-pyrido[3,4-b]indol-7-yloxy)ethyl 4-methylbenzene sulfonate, was prepared. Attempts to label this precursor resulted in decomposition of the precursor and no labeling was obtained. An explanation of this behavior is may be the high reactivity of the toluenesulfonyl leaving group used. As a consequence, the radiosynthesis of [^{18}F]fluoroethyl harmol was performed in a two-step procedure, comparable to [^{18}F]F- d_2 -MH. The labeling agent used in this route, 2-[^{18}F]FETos, was prepared on a self-made automated synthesis module, yielding a radiochemical yield of about 60% after 55 min. The [^{18}F]FETos, trapped on a SPE cartridge

during the final step of the automated synthesis, was eluted with DMSO and tempered to the reaction temperature. Then it was reacted with a solution of harmol and 5 N NaOH in DMSO, to obtain the [^{18}F]FEH. The reaction parameters of this ^{18}F -fluorethylation were optimized, resulting in the following conditions: 15 μmol precursor, 5.6 μL NaOH, 110 $^{\circ}\text{C}$ and 20 min reaction time. Using these conditions radiochemical yield of up to 95% could be achieved. Purification of the reaction mixture was performed in an analogue manner to [^{18}F]F- d_2 -MH, yielding the [^{18}F]FEH in an overall radiochemical yield of $47 \pm 2\%$ after a synthesis time of 105 min and specific activities of 40–90 GBq/ μmol . Although, this two-step procedure results in a longer synthesis time, it finally produces slightly higher yields of [^{18}F]FEH and seems to be robust, compared to the method published by Blom et al.²⁷

In contrast to [^{18}F]F- d_2 -MH and [^{18}F]FEH, the labeling of the PEGylated harmol derivatives was achieved via direct ^{18}F -fluorination of the tosylated precursors. The tosylated precursors gave higher yields than the halogenated precursors used in the study of Blom et al.²⁷ To obtain the basic conditions, which are needed for ^{18}F -direct fluorination, a potassium carbonate/Kryptofix[®] 2.2.2. system was used. However, first attempts to label the precursor using different solvents and temperatures resulted in low radiochemical yields, which may be explained by the acidic indole hydrogen hampering the labeling reaction. Hence, in the next experiments the ratio of precursor to potassium carbonate/Kryptofix[®] 2.2.2. was raised from 1/1 to 1/4.3, resulting in higher radiochemical yields of up to 20% in DMF. These high base concentrations did not only increase the conversion, but also reduced the reliability of the labeling, resulting in more by-products and a more complicated purification of the tracers. Therefore, as an alternative route to the conventional heating, a microwave-assisted synthesis was tested. During the first experiments, using potassium carbonate/Kryptofix[®] 2.2.2., it was observed, that higher radiochemical yields were obtained compared to the conventional heating and side products could be minimized. Hence, this method was screened regarding to temperature, which had the biggest impact on conversion rates, cf. Table 3. Reaction times and amount of precursor seemed not to be major rate limiting parameters (data not shown).

The optimization of this direct ^{18}F -fluorination showed, that DMF or DMSO resulted in no or low radiochemical yields, whilst MeCN gave radiochemical yields of up to 50% and thus was chosen for the next steps. Subsequently, the reaction temperature was screened giving the highest RCY between 100–135 $^{\circ}\text{C}$. When the temperature was raised beyond that range decomposition of the precursor increased drastically, while lowering it beyond that range resulted in very low radiochemical yields. Additionally, the precursor concentration was screened showing the highest RCY with a precursor concentration of at least 12.5 $\mu\text{mol}/\text{mL}$. Finally, the influence of the reaction time on the RCY was investigated showing the highest RCY in a time range of 1–6 min of microwave

heating. Longer reaction times led to decomposition of all precursors. After the optimization, the purification of the tracers was performed in an analogue manner to [^{18}F]F- d_2 -MH, yielding [^{18}F]11a–c in an overall radiochemical yield of $20 \pm 10\%$ after a synthesis time of 85 min.

3.3. Plasma stability tests

Plasma stability is an important issue for PET-tracers, since a fast metabolism in the plasma reduces drastically the tracer-uptake target regions. For brain tracers this circumstance is even more crucial if non-polar metabolites are formed, increasing unspecific binding and complicating the kinetic modeling of the tracer. Thus, all tracers were incubated in human serum, the plasma proteins were precipitated by addition of MeCN and separated by centrifugation. The obtained supernatant was analyzed by HPLC, to determine the stability of the respective tracer in vitro, showing that all tracers had a sufficient stability over an observation period of 60 min. The results of this study are shown in Table 4.

3.4. In vivo imaging studies in Sprague Dawley rats

To determine brain uptake kinetics of the ^{18}F -fluorinated harmol derivatives, μPET studies in Sprague Dawley rats were performed. Furthermore, for [^{18}F]F- d_2 -MH and [^{18}F]FEH the selectivity of the tracers was investigated by a selective blocking of MAO B and MAO A. In a first imaging study the brain uptake of [^{18}F]F- d_2 -MH in untreated, in ι -deprenyl treated and in clorgyline treated animals was measured (Fig. 3).

[^{18}F]F- d_2 -MH showed a high initial uptake and rapid clearance out of the brain. The initial SUV of 2.1 ± 0.4 g/mL after 10 s decreased to 1.2 ± 0.2 g/mL within 30 min, which can be assigned to blood flow. The highest uptake levels of 3.7 ± 0.5 g/mL were reached 90 s p.i., followed by a fast washout to 1.5 ± 0.2 g/mL after 20 min and 1.0 ± 0.2 g/mL after 45 min. Blocking of MAO B was performed using ι -deprenyl, a selective MAO B inhibitor, following a procedure described in the literature.²⁶ The uptake kinetics of treated animals showed a behavior very similar to the untreated animals, hence a high initial uptake and fast clearance out of the brain. The highest uptake values of 3.8 ± 0.8 g/mL were reached at 50 s p.i., followed by washout to 1.4 ± 0.5 g/mL after 20 min and 0.9 ± 0.2 g/mL after 45 min. At later time points a slightly lower uptake, compared to the untreated animals, was observed, but under consideration of the errors of both groups there is no significant difference. Finally, blocking of the MAO A was done using clorgyline a selective MAO A inhibitor.²⁰ These animals showed very similar initial brain uptake of 3.8 ± 0.6 g/mL, but in contrast to the other two groups a faster washout was observed, giving SUVs of 1.0 ± 0.2 g/mL after 20 min. The highest differences in brain uptake between the untreated and the clorgyline-treated animals, representing the specific binding, were observed from 3 to 20 min p.i., giving SUV differences of >0.5 g/mL. In summary, both blocking studies indicate, that [^{18}F]F- d_2 -MH binds selective to MAO A albeit it possesses very fast pharmacokinetics in vivo.

Table 3
Optimization of ^{18}F -labeling of **2** and **7a–c**

Temp ($^{\circ}\text{C}$)	Tracer		
	11a	11b	11c
115 ^a	3%	10%	2%
120 ^b	5%	47%	10%
125 ^a	$32 \pm 6\%$	$39 \pm 11\%$	$46 \pm 2\%$
135 ^a	28%	15%	38%
140 ^b	nd	nd	nd

For optimization of the reaction temperature the optimized precursor and base concentrations were used.

^a Microwave assisted heating.

^b Conventional heating.

Table 4

Stability of the ^{18}F -fluorinated harmol derivatives in human plasma as a function of the incubation time at 37 $^{\circ}\text{C}$

Incubation time	5 min	15 min	30 min	60 min
[^{18}F]F- d_2 -MH	95.5 ± 1.9	95.8 ± 0.1	95.8 ± 0.1	94.4 ± 0.1
[^{18}F]FEH	98.6 ± 2.9	98.4 ± 2.8	97.9 ± 2.8	97.5 ± 2.5
[^{18}F]PEG2-harmol	96.0 ± 1.8	97.2 ± 1.4	96.7 ± 1.6	94.7 ± 1.9
[^{18}F]PEG3-harmol	95.4 ± 0.2	97.0 ± 0.4	95.4 ± 2.3	95.7 ± 1.4
[^{18}F]PEG4-harmol	97.8 ± 0.6	97.1 ± 1.1	98.0 ± 0.9	97.0 ± 0.7

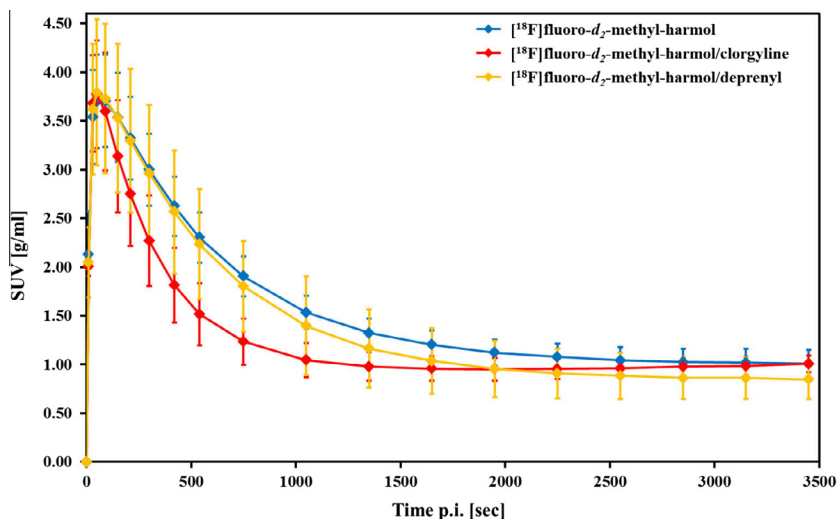


Figure 3. Time activity curves from microPET-studies of [^{18}F]- d_2 -MH. Curves were drawn from activity measurements in the brain for untreated ($n = 5$), cloglyline-treated ($n = 3$) and deprenyl-treated ($n = 3$) Sprague Dawley rats. Each curve gives the mean SUV \pm SEM.

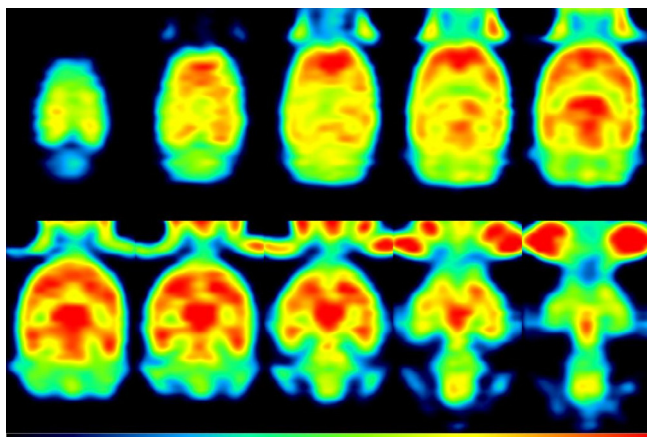


Figure 4. Representative horizontal brain slices of the brain uptake of [^{18}F]- d_2 -MH in Sprague Dawley rats. This series of OSEM3d reconstructed images (dorsal to ventral, slice interval 1.0 mm) shows a sum image from 0–12.5 min p.i. (color code: 80–170 kBq/g).

Representative images for the early distribution pattern of [^{18}F]- d_2 -MH in the rat brain are shown in Figure 4. Besides the high uptake in the brain, a high uptake in the harderian glands (upper left and right corner of each image) was also observed. Furthermore, a high accumulation in the skull was noticed in all three groups of animals at later time points, although the plasma stability test of the tracer showed a high stability in human serum. This indicates tracer metabolism under release of [^{18}F]fluoride, a highly sensitive bone-seeking radionuclide, which accumulates in skull.⁴³

For [^{18}F]FEH the μ PET studies were done using a similar setup to [^{18}F]- d_2 -MH, resulting in SUV curves shown in Figure 5. For the untreated animals a high initial uptake, comparable to [^{18}F]- d_2 -MH, was observed followed by a slower washout from the brain. Highest SUV of [^{18}F]FEH of 3.7 ± 0.4 g/mL was reached at 7 min p.i., followed by a slow clearance out of the brain resulting in 3.6 ± 0.4 g/mL after 20 min and 3.4 ± 0.4 g/mL after 45 min, respectively.

Additionally, the selectivity of **10** was investigated in blocking studies using ι -deprenyl and cloglyline. ι -Deprenyl-blocked rats

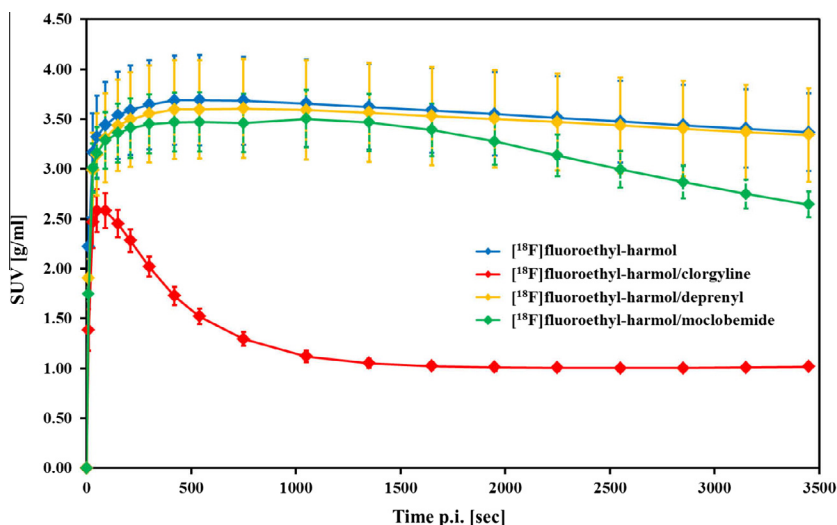


Figure 5. Time activity curves from microPET-studies of [^{18}F]FEH. Curves were drawn from activity measurements in the whole brain in untreated and cloglyline- and deprenyl-treated Sprague Dawley rats. Each curve gives the mean SUV \pm SEM.

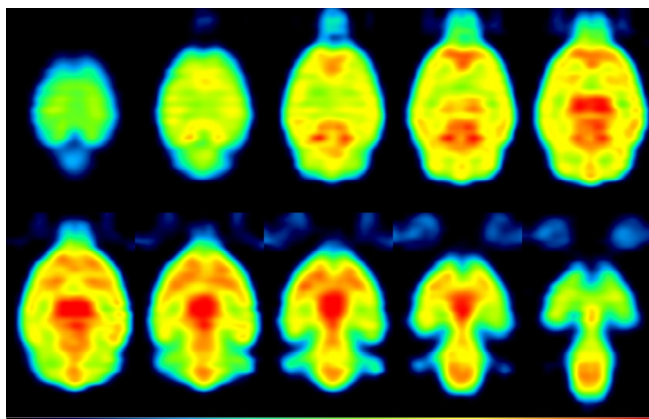


Figure 6. Representative horizontal brain slices of the brain uptake of $[^{18}\text{F}]\text{FEH}$ in Sprague Dawley rats. This series of OSEM3d reconstructed images (dorsal to ventral, slice interval 1.0 mm) shows a sum image from 30–60 min p.i. (color code: 200–650 kBq/g).

showed nearly identical SUV-normalized uptake curves as the untreated animals. Thus, a high initial uptake was followed by a slow washout from the brain. Highest uptake of 3.6 ± 0.5 g/mL was achieved at 7 min p.i., followed by a slow clearance giving SUVs of 3.6 ± 0.5 g/mL after 20 min and 3.4 ± 0.5 g/mL after 45 min. These results indicate that $[^{18}\text{F}]\text{FEH}$ does not bind to MAO B. In contrast, blocking with clorgyline showed a significantly different uptake curve compared to the untreated rats. Following a moderate initial uptake of the tracer in the brain, a rapid clearance was observed, showing a maximum SUV of 2.6 ± 0.5 g/mL after 50 s and SUVs of 1.1 ± 0.2 and 1.0 ± 0.03 g/mL after 20 and 45 min. Hence, the binding of $[^{18}\text{F}]\text{FEH}$ can be drastically reduced by an MAO A inhibitor. This clearly shows the high selectivity of the tracer for MAO A.

Finally, challenge experiments using moclobemide were performed, to determine the reversibility of the $[^{18}\text{F}]\text{FEH}$ binding to MAO A. Following a published procedure, moclobemide was applied in two bolus injections at 20 min and 45 min p.i. of the tracer. As shown in Figure 5, the first application of moclobemide directly results in a slight increase of the radioactivity in the brain. This effect can be explained by the clearance of $[^{18}\text{F}]\text{FEH}$ from the peripheral organs with high MAO A concentrations, like heart, liver or pancreas. This clearance results in a higher tracer concentration

in the blood and consequently an increased radioactivity signal in the brain. Following this slight increase, a significant washout, compared to the untreated rats was observed, demonstrating the reversibility of the $[^{18}\text{F}]\text{FEH}$ binding. In summary, these experiments demonstrate promising properties of $[^{18}\text{F}]\text{FEH}$ for the visualization of the MAO A status in vivo, showing high affinity, high selectivity and the reversibility of the tracer to MAO A.

Although the MAO A is ubiquitous expressed in the brain, for some regions a higher uptake of $[^{18}\text{F}]\text{FEH}$ was observed. These regions include cortical regions, the thalamus, the colliculus inferior and the midbrain. Interestingly, for the cerebellum, a brain region with a low concentration of MAO A, a moderate uptake was determined. An explanation for this behavior could be that the locus coeruleus, a region with one of the highest MAO A expressions in brain, is directly located next to the grey matter of the cerebellum, which results, via spill-over effects, in an increased apparent uptake in the cerebellum. Representative images for the distribution pattern of $[^{18}\text{F}]\text{FEH}$ in the rat brain, are shown in Figure 6. The relatively high MAO A concentrations in most brain regions aggravate an exact determination of the SUVs, due to partial volume and spill-over effects from neighboring regions. Thus, a detailed determination of the SUVs for the different brain regions was not performed.

The evaluation of the brain uptake of the ^{18}F -PEGylated harmol derivatives, $[^{18}\text{F}]\text{PEG2-harmol}$, $[^{18}\text{F}]\text{PEG3-harmol}$ and $[^{18}\text{F}]\text{PEG4-harmol}$, μPET studies in untreated Sprague Dawley rats were performed. Surprisingly, none of these tracers showed a significant brain uptake. In the previous work from Blom et al., however, it was demonstrated in autoradiographic studies, that two of these derivatives, $[^{18}\text{F}]\text{PEG2-harmol}$ and $[^{18}\text{F}]\text{PEG3-harmol}$, bind to MAO A and also show a high selectivity for this target. Hence, the most likely explanation for this behavior is that the PEGylation results in a reduction of the lipophilicity of these compounds, which hinders their passage of the blood–brain barrier. To investigate the differences in lipophilicity we determined the capacity factors (k') for all the derivatives ending up with the following order: $[^{18}\text{F}]\text{FEH}$: $k' = 4.03 > [^{18}\text{F}]\text{-}d_2\text{-MH}$: $k' = 4.01 > [^{18}\text{F}]\text{PEG2-harmol}$: $k' = 3.97 > [^{18}\text{F}]\text{PEG3-harmol}$: $k' = 3.77 > [^{18}\text{F}]\text{PEG4-harmol}$: $k' = 3.74$. Thus, $[^{18}\text{F}]\text{FEH}$ is the most lipophilic compound of the derivatives, whereas the lipophilicity decreases due to PEGylation. This order is in accordance with the experimental observation that the brain uptake of the PEGylated compounds, although very low, decreases further from $[^{18}\text{F}]\text{PEG2-harmol}$ to $[^{18}\text{F}]\text{PEG4-harmol}$. Besides the lower lipophilicity of the PEGylated compounds, the

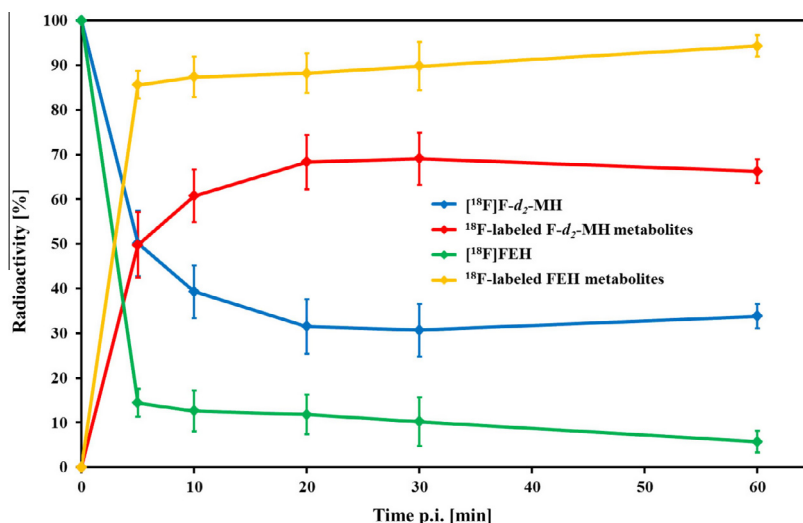


Figure 7. Metabolism of $[^{18}\text{F}]\text{F-}d_2\text{-MH}$ and $[^{18}\text{F}]\text{FEH}$ in Sprague Dawley rats as a function of time post injection

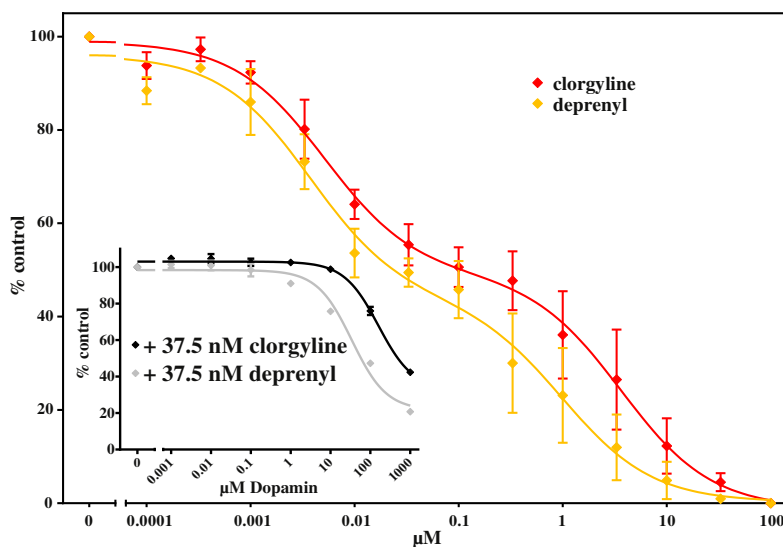


Figure 8. Dose–response curves of clorgyline and *l*-deprenyl against MAO activity in vitro and determination of the IC_{50} values of dopamine against MAO A and MAO B. Clorgyline and *l*-deprenyl were co-incubated at concentrations ranging from 0.1 nM up to 100 μ M. The IC_{50} values obtained were 3.1 nM ($\lg IC_{50}$: -2.5 ± 0.3 ($\lg \mu$ M)) and 3.0 μ M ($\lg IC_{50}$: 0.47 ± 0.31 ($\lg \mu$ M)) for clorgyline (squares) at the high and low affinity sites, respectively. The IC_{50} values obtained were 3.2 nM ($\lg IC_{50}$: -2.50 ± 0.23 ($\lg \mu$ M)) and 1.0 μ M ($\lg IC_{50}$: -0.019 ± 0.375 ($\lg \mu$ M)) for deprenyl (triangles) at the high and low affinity sites, respectively. $n = 4$. The fractions of the high affinity sites amounted to $46 \pm 5\%$ and $52 \pm 4\%$ for clorgyline and *l*-deprenyl, respectively.

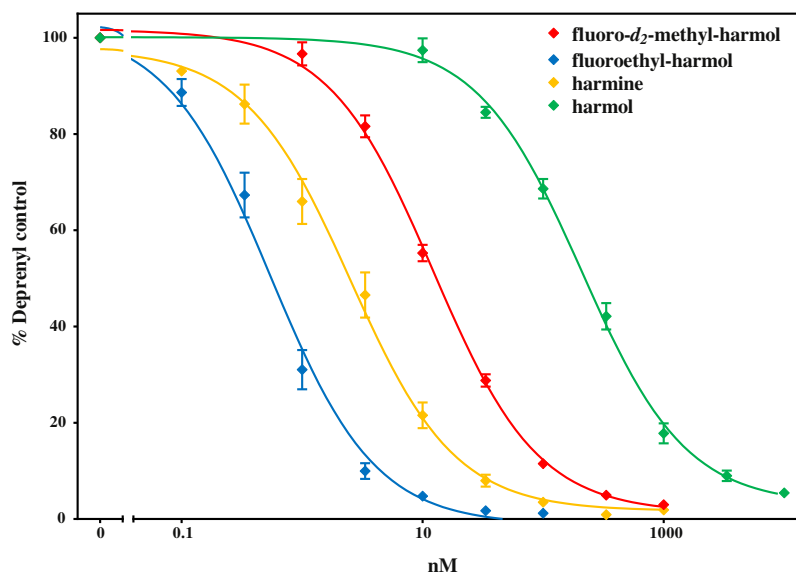


Figure 9. MAO A activity of harmol, harmine, *F*-*d*₂-MH and FEH. The ranges of concentrations were between 0.1 nM and 100 nM for harmine and FEH, between 1 nM and 1 μ M for *F*-*d*₂-MH, and between 10 nM and 10 μ M for harmol. The corresponding IC_{50} values are given in the text.

capability of the PEG-chains to form H-bonds may be responsible for the low brain uptake. Since each pair of hydrogen bonds formed with the solvent results in a 10-fold decrease in membrane permeation, this limits the ability of the PEGylated compounds to pass penetrate the BBB with increasing length of the PEG-chain.^{44,45} Due to these results no further in vivo experiments were performed with these compounds.

3.5. In vivo metabolism studies

In the in vivo imaging studies of [¹⁸F]*F*-*d*₂-MH a high accumulation of activity in the skull was observed at later time points, indicating a metabolism of the tracer under release of [¹⁸F]fluoride.

Hence, the metabolic profile of [¹⁸F]*F*-*d*₂-MH was examined in four animals, resulting in the data depicted in Figure 7. In contrast to the in vitro experiments, the tracer undergoes a fast in vivo metabolism showing only 50% of intact tracer after 5 min, which gets further metabolized, resulting in only 30% of intact tracer after 20 min p.i.. HPLC analysis of the plasma water showed exclusively polar metabolites having retention times comparable to the dead time of the HPLC. This underlines the hypothesis that this tracer is metabolized under release of [¹⁸F]fluoride.

In a further evaluation the metabolic profile of the [¹⁸F]FEH was examined in an analogous manner to [¹⁸F]*F*-*d*₂-MH, cf Figure 7. In comparison to the ¹⁸F-fluoromethylated compound, a fast in vivo

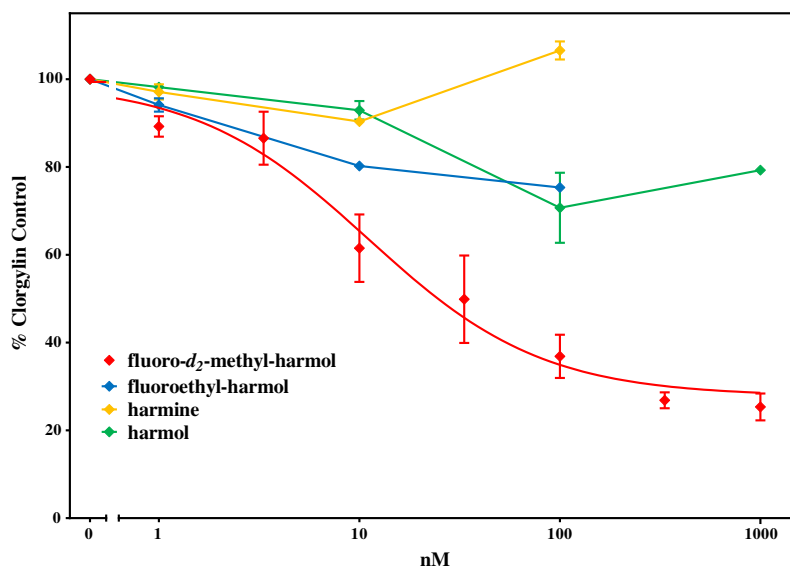


Figure 10. MAO B activity of harmol, harmine, F-*d*₂-MH and FEH. The ranges of concentrations were between 1 and 100 μ M for harmine and FEH and between 1 μ M and 1 mM for harmol and F-*d*₂-MH.

metabolism was observed as well, showing only 15% of intact tracer after 5 min, which gets further metabolized, resulting in only 5% of intact tracer after 60 min p.i.. HPLC analysis of the plasma water showed two different polar metabolites having retention times slightly higher than the dead time of the HPLC, but no defluorination could be observed.

3.6. Monoamine oxidase assays

Based on the results of the in vivo imaging studies, potential ligands, namely [¹⁸F]F-*d*₂-MH and [¹⁸F]FEH, were evaluated in enzyme assays to determine their affinity towards MAO-A and MAO-B. To verify the validity of the MAO assay, dopamine was assayed in the presence of clorgyline and *l*-deprenyl (MAO B) in order to obtain the specific MAO A activity, respectively (Fig. 8, insert).

The calculated IC₅₀ were 34 ± 7 μ M and 160 ± 23 μ M, respectively, matching with the published K_M value of 285 μ M using [³H]dopamine as substrate and PC12 cells as source of total MAO activity.⁴⁶ The amount to block MAO A activity decreased in the order FEH, harmine, F-*d*₂-MH and harmol (Fig. 9) with a range from 0.54 ± 0.06 nM for FEH to 208 ± 16 nM for harmol. Still, the IC₅₀ value for harmine (2.5 ± 0.3 nM) and F-*d*₂-MH (12.2 ± 0.6 nM) were in the low nanomolar range.

Clorgyline and *l*-deprenyl (37.5 nM each) were used to specifically inhibit MAO A and MAO-B activity. These concentrations were the mid points between the Ig IC₅₀ values of the two respective dose–response curves (Fig. 8), allowing to monitor effectively and precisely the MAO B and MAO A activities as the IC₅₀ values differ by at least 300-fold.

The MAO-B activity of harmol, harmine and FEH was negligible in the solubility range (Fig. 10). F-*d*₂-MH displayed an IC₅₀ of 11 ± 4 μ M, nearly 1000-fold lower than for MAO A. Harmol, harmine and FEH are highly MAO A selective compounds, whereas F-*d*₂-MH, surprisingly, substantially inhibited MAO-B though with a 1000-fold lower potency (11 ± 4 μ M and 12.2 ± 0.6 nM for MAO-B and MAO A, respectively). Moreover, the F-*d*₂-MH efficacy was only 78% to inhibit MAO B in contrast to the action against MAO A, which amounted to nominally 100% for all compounds tested. The differences in the washout between F-*d*₂-MH and FEH in the

presence of clorgyline and *l*-deprenyl (Figs. 3 and 5) may be reflected in the in vitro selectivities (Figs. 9 and 10). The IC₅₀ values of FEH were the highest we observed (0.54 ± 0.06 nM). This high affinity may account for the slow washout compared to that of F-*d*₂-MH.

4. Conclusion

In the present work five ¹⁸F-labeled harmine derivatives were evaluated in μ PET studies to determine their suitability to visualize the MAO A status in vivo. The organic syntheses of the precursors and the reference compounds were established and optimized. For radiolabeling of [¹⁸F]F-*d*₂-MH and [¹⁸F]FEH a two-step procedure was chosen. Both compounds were obtained after synthesis times from 85 to 115 min in high RCY of about 30–47%. Using toluenesulfonyl leaving groups and a microwave-supported radiosynthesis it was possible to increase the RCY of the direct ¹⁸F-fluorinations of the PEGylated harmol compounds up to 45%. Plasma stability tests in human serum showed that all tracers are stable over an incubation time of 60 min, showing 95% or higher for the unbound intact tracer. Surprisingly, the ¹⁸F-labeled PEGylated compounds showed no significant brain uptake in first μ PET studies. A possible reason for this behavior might be the reduced lipophilicity and an increased formation of H-bonds caused by the PEGylation, thus preventing the passage of the blood–brain barrier. In contrast, [¹⁸F]F-*d*₂-MH showed a high brain uptake and a good specificity, albeit this was also accompanied by a fast pharmacokinetic profile. μ PET studies performed for [¹⁸F]FEH showed that [¹⁸F]FEH revealed very promising properties for the in vivo visualization of the MAO A, like high brain uptake, high specificity to MAO A and reversibility of binding. In MAO binding assays a high affinity for the MAO A was observed for F-*d*₂-MH and FEH, showing IC₅₀ values of 12.2 ± 0.6 nM and 0.54 ± 0.06 nM, respectively. Surprisingly, F-*d*₂-MH also inhibited the MAO-B, though with a 1000-fold lower potency (IC₅₀(MAO-B): 11 ± 4 μ M). It remains to be evaluated whether the increase in affinity from harmol over F-*d*₂-MH to FEH can be extended to fluoro-butyl-harmine and fluoro-*t*-butyl-harmine. Although [¹⁸F]F-*d*₂-MH showed very fast pharmacokinetics in in vivo imaging studies, it is nevertheless a potential candidate for MAO-A imaging, since it has been shown that

species differences between animals and humans can drastically influence the pharmacokinetics of a tracer.²⁴ Hence, for both compounds, [¹⁸F]F-d₂-MH and [¹⁸F]FEH, a further evaluation is indicated.

Acknowledgments

This work was supported by the research cluster SAMT of the Johannes Gutenberg-University Mainz. We thank Kerstin Lüddens-Dämgen for technical assistance.

References and notes

- Hare, M. L. C. *Biochem. J.* **1928**, *22*, 879.
- Zeller, E. A. *Helv. Chim. Acta* **1937**, *21*, 880.
- Finberg, J. P. M.; Gillman, K. *Int. Rev. Neurobiol.* **2011**, *100*, 169.
- Shih, J. C.; Chen, K.; Ridd, M. J. *Annu. Rev. Neurosci.* **1999**, *22*, 197.
- Lan, N. C.; Chen, C. H.; Shih, J. C. *J. Neurochem.* **1989**, *52*, 1652.
- Bach, A. W.; Lan, N. C.; Johnson, D. L.; Abell, C. W.; Bembenek, M. E.; Kwan, S. W.; Seeburg, P. H.; Shih, J. C. *Proc. Natl. Acad. Sci. U.S.A.* **1988**, *85*, 4934.
- Tong, J.; Meyer, J. H.; Furukawa, Y.; Boileau, I.; Chang, L. J.; Wilson, A. A.; Houle, S.; Kish, S. J. *J. Cereb. Blood Flow Metab.* **2013**, *33*, 863.
- Strolin Benedetti, M.; Dostert, P.; Tipton, K. F. *Dev. Pharmacol. Ther.* **1992**, *18*, 191.
- Tsang, D.; Ho, K. P.; Wen, H. L. *Dev. Neurosci.* **1986**, *8*, 243.
- Nicotra, A.; Pierucci, F.; Parvez, H.; Senatori, O. *Neurotoxicology* **2004**, *25*, 155.
- Kalgutkar, A. S.; Dalvie, D. K.; Castagnoli, N.; Taylor, T. J. *Chem. Res. Toxicol.* **2001**, *14*, 1139.
- Ginovart, N.; Meyer, J. H.; Boovariwala, A.; Hussey, D.; Rabiner, E. A.; Houle, S.; Wilson, A. A. *J. Cereb. Blood Flow Metab.* **2006**, *26*, 330.
- Livingston, M. G.; Livingston, H. M. *Drug Saf.* **1996**, *14*, 219.
- Cohen, G. J. *Neural Transm. Suppl.* **1990**, *32*, 229.
- Youdim, M. B. H.; Edmondson, D.; Tipton, K. F. *Nat. Rev. Neurosci.* **2006**, *7*, 295.
- Vaya, J.; Aluf, Y.; Finberg, J. P. M. In *Oxidative Stress and Free Radical Damage in Neurology*; Gadoth, N., Gobel, H. H., Eds.; Springer: New York, 2012; pp 191–224.
- Da Prada, M.; Zürcher, G.; Wüthrich, I.; Haefely, W. E. *J. Neural Transm. Suppl.* **1988**, *26*, 31.
- Blob, L. F.; Sharoky, M.; Camobell, B. J.; Kemper, E. M.; Gilmor, M. G.; VanDenberg, C. M. *CNS Spectr.* **2007**, *12*, 25.
- Stahl, S. M.; Felker, A. *CNS Spectr.* **2008**, *13*, 855.
- Bergström, M.; Westerberg, G.; Långström, B. *Nucl. Med. Biol.* **1997**, *24*, 287.
- Ametamey, S. M.; Beer, H.; Antonini, A.; Leenders, K. L.; Schubiger, P. A. *Nucl. Med. Biol.* **1996**, *23*, 229.
- Kerseman, K.; Van Laeken, N.; De Vos, F. *J. Labelled Compd. Radiopharm.* **2013**, *56*, 78.
- Dolle, F.; Valette, H.; Bramoulle, Y.; Guenther, I.; Fuseau, C.; Coulon, C.; Lartizien, C.; Jegham, S.; George, P.; Curet, O.; Pinquier, J.-L.; Bottlaender, M. *Bioorg. Med. Chem. Lett.* **2003**, *13*, 1771.
- Fowler, J. S.; Ding, Y. S.; Logan, J.; MacGregor, R. R.; Shea, C.; Garza, V.; Gimi, R.; Volkow, N. D.; Wang, G. J.; Schlyer, D.; Ferrieri, R.; Gatley, S. J.; Alexoff, D.; Carter, P.; King, P.; Pappas, N.; Arnett, C. D. *Nucl. Med. Biol.* **2001**, *28*, 779.
- Kim, H.; Sablin, S. O.; Ramsay, R. R. *Arch. Biochem. Biophys.* **1997**, *337*, 137.
- Bergström, M.; Westerberg, G.; Kihlberg, T.; Långström, B. *Nucl. Med. Biol.* **1997**, *24*, 381.
- Blom, E.; Karimi, F.; Eriksson, O.; Hall, H.; Långström, B. *J. Labelled Compd. Radiopharm.* **2008**, *51*, 277.
- Smart, B. E. *J. Fluorine Chem.* **2001**, *109*, 3.
- Müller, K.; Faeh, C.; Diederich, F. *Science* **2007**, *317*, 1881.
- Bell, R. P. *Chem. Soc. Rev.* **1973**, *3*, 513.
- Zhang, M.-R.; Maeda, J.; Ito, T.; Okauchi, T.; Ogawa, M.; Noguchi, J.; Suhara, T.; Halldin, C.; Suzuki, K. *Bioorg. Med. Chem.* **2005**, *13*, 1811.
- Beyerlein, F.; Piel, M.; Höhnemann, S.; Rösch, F. *J. Labelled Compd. Radiopharm.* **2013**, *56*, 360.
- Block, D.; Knochel, A.; Hamburg, U.; Beckmann, R. *J. Labelled Compd. Radiopharm.* **1986**, *23*, 467.
- Mohler, D. L.; Shen, G. *Org. Biomol. Chem.* **2006**, *4*, 2082.
- Riss, P. J.; Hoehnemann, S.; Piel, M.; Roesch, F. *J. Labelled Compd. Radiopharm.* **2013**, *56*, 356.
- Ucar, G. *Hacettepe Univ. Eczacilik Fak. Derg.* **2004**, *24*, 25.
- Bergström, M.; Westerberg, G.; Németh, G.; Traut, M.; Gross, G.; Greger, G.; Müller-Peltzer, H.; Safer, A.; Eckernäs, S. A.; Grahner, A.; Långström, B. *Eur. J. Clin. Pharmacol.* **1997**, *52*, 121.
- Herth, M. M.; Debus, F.; Piel, M.; Palner, M.; Knudsen, G. M.; Lüddens, H.; Rösch, F. *Bioorg. Med. Chem. Lett.* **2008**, *18*, 1515.
- Lüddens, H.; Lang, H. J.; Korpi, E. R. *Eur. J. Pharmacol.* **1998**, *344*, 269.
- Krajl, M. *Biochem. Pharmacol.* **1965**, *14*, 1684.
- Lueddens, H. W.; Newman, A. H.; Rice, K. C.; Skolnick, P. *Mol. Pharmacol.* **1986**, *29*, 540.
- Gabay, S.; Achee, F. M.; Mentes, G. J. *Neurochem.* **1976**, *27*, 415.
- Harmer, C. L.; Burns, J. E.; Sams, A.; Spittle, M. *Clin. Radiol.* **1969**, *20*, 204.
- Pardridge, W. M. *J. Cereb. Blood Flow Metab.* **2012**, *32*, 1959.
- Stein, W. D. *The Molecular Basis of Diffusion Across Cell Membranes*; Academic Press: New York, NY, 1967; pp 66–125.
- Youdim, M. B.; Heldman, E.; Pollard, H. B.; Fleming, P.; McHugh, E. *Neuroscience* **1986**, *19*, 1311.